Magnetic Resonance in Medicine 57:1027–1036 (2007)

Temporally Constrained Reconstruction of Dynamic Cardiac Perfusion MRI

Ganesh Adluru,[1–3] Suyash P. Awate,[2] Tolga Tasdizen,[2] Ross T. Whitaker,[2] and Edward V.R. DiBella[3,4]*

Dynamic contrast-enhanced (DCE) MRI is a powerful technique to probe an area of interest in the body. Here a temporally constrained reconstruction (TCR) technique that requires less *k*-space data over time to obtain good-quality reconstructed images is proposed. This approach can be used to improve the spatial or temporal resolution, or increase the coverage of the object of interest. The method jointly reconstructs the space-time data iteratively with a temporal constraint in order to resolve aliasing. The method was implemented and its feasibility tested on DCE myocardial perfusion data with little or no motion. The results obtained from sparse *k*-space data using the TCR method were compared with results obtained with a sliding-window (SW) method and from full data using the standard inverse Fourier transform (IFT) reconstruction. Acceleration factors of 5 (R = 5) were achieved without a significant loss in image quality. Mean improvements of 28 ± 4% in the signal-to-noise ratio (SNR) and 14 ± 4% in the contrast-to-noise ratio (CNR) were observed in the images reconstructed using the TCR method on sparse data (R = 5) compared to the standard IFT reconstructions from full data for the perfusion datasets. The method has the potential to improve dynamic myocardial perfusion imaging and also to reconstruct other sparse dynamic MR acquisitions. Magn Reson Med 57:1027–1036, 2007. © 2007 Wiley-Liss, Inc.

Key words: dynamic contrast-enhanced MR; cardiac perfusion; regularization; regularization parameter; L-curve

Dynamic contrast-enhanced (DCE) MRI is used to track changes over time in an object of interest by acquiring a series of images. A contrast agent is injected and the data are acquired in *k*-space for each time frame. Rapid acquisitions are required to track the quickly changing contrast in the object. One application of DCE-MRI is myocardial perfusion, which is an important tool for assessing coronary artery disease. In DCE-MRI for myocardial perfusion, contrast agents such as gadolinium (Gd)-DTPA are injected and images are acquired using ECG-gated sequences to track the uptake of the contrast agent by the myocardium at high temporal resolution.

To reduce the data acquisition time of dynamic MRI, a number of techniques have been developed. These methods acquire a fraction of *k*-space in each time frame and reconstruct images based on a priori information about the dynamic data. Methods such as keyhole imaging (1,2) and reduced-encoding MR imaging with generalized-series reconstruction (RIGR) (3–5) assume that in a dynamic sequence only the low-frequency data change and the high-frequency data remain static. Thus full data can be acquired for a single frame in the sequence and only low-frequency data need to be acquired for the remaining frames. This assumption of static high frequencies is not always accurate.

View-sharing-type methods (6–9) assume that the dynamics in an image sequence change only by a small amount from frame to frame. Thus only a fraction of data can be acquired for each frame and the missing data can be obtained from the adjacent frames. Such data-sharing is equivalent to linear interpolation in time and can reduce temporal resolution.

More recently, Madore et al. (10) proposed the unaliasing by Fourier-encoding the overlaps using the temporal dimension (UNFOLD) method for cardiac cine imaging and functional MRI (fMRI). UNFOLD uses efficient encoding of the *k-t* space to reduce the number of acquired lines in the phase-encode direction for each time frame. The method achieved a speed-up factor of 2 for cardiac cine imaging. The *k-t* broad-use linear acquisition speed-up technique (BLAST) proposed by Tsao et al. (11) uses spatiotemporal correlations and low-resolution training data to achieve net acceleration factors of 4.1–4.3 (12,13) for 3D cardiac cine imaging. Furthermore, *k-t* BLAST and UNFOLD can be combined with parallel imaging techniques (14,15) based on multiple receive coils to improve image quality or acquisition speed (11,16).

For myocardial perfusion, higher acceleration factors usually cannot be achieved using UNFOLD due to the large amount of variation of contrast in images, which requires more temporal bandwidth. *k-t* BLAST has been used predominantly to speed up cardiac cine imaging (11–13,17,18) and is typically used with additional training data to capture correlation information. In addition, the UNFOLD and *k-t* BLAST methods are typically used for data undersampled in an interleaved fashion. To overcome some of the limitations of the previously proposed methods in terms of temporal bandwidth and requiring additional training data, and to further improve the reconstruction from sparse data, we propose an inverse problem approach (19) with temporal constraints.

[1]Electrical and Computer Engineering Department, University of Utah, Salt Lake City, Utah, USA.

[2]Scientific Computing and Imaging Institute, School of Computing, University of Utah, Salt Lake City, Utah, USA.

[3]Utah Center for Advanced Imaging Research, Department of Radiology, University of Utah, Salt Lake City, Utah, USA.

[4]Department of Bioengineering, University of Utah, Salt Lake City, Utah, USA.

*Correspondence to: Edward DiBella, Ph.D., UCAIR/Radiology, 729 Arapeen Dr., Salt Lake City, UT 84108. E-mail: Ed@ucair.med.utah.edu

Received 7 September 2006; revised 30 January 2007; accepted 28 February 2007.

DOI 10.1002/mrm.21248
Published online in Wiley InterScience (www.interscience.wiley.com).

MATERIALS AND METHODS

Temporally Constrained Reconstruction (TCR) Method

The standard approach to reconstructing dynamic images from full *k*-space data is to apply a 2D inverse Fourier transform (IFT) on each time frame of data. Acquiring less data in *k*-space for each time frame (*k-t* space) results in aliasing in the image space and temporal frequency spectrum (*x-f* space). Pixels from different positions in *x-f* space overlap onto a single pixel, making the problem of reconstruction ill posed. If general a priori information is known about the data, this can be incorporated into an iterative reconstruction to resolve the aliasing. The main idea of the TCR method proposed here is to use an appropriate temporal model as a constraint on the reconstruction in order to remove the artifacts from undersampling and to preserve or increase the signal-to-noise ratio (SNR).

The theory presented here parallels the regularization theory that is often used to solve ill-posed inverse problems. The standard discrete IFT reconstruction from full *k*-space data can be mathematically represented as

$$d = Fm \qquad [1]$$

where d represents the full data acquired in *k*-space for different time frames; m represents complex image data, which is the corresponding series of images for the time frames; and F represents the 2D-FT on each time frame in the dynamic sequence. When full *k*-space data d are undersampled, and only sparse data, $\tilde{d}$, are acquired, aliasing occurs in the *x-f* space (11). A solution, $\hat{m}$, that resolves the aliasing can be obtained by finding a balance between fidelity to the acquired sparse data and incorporating an additional constraint in terms of a temporal model that is satisfied by the full data. Reconstruction can be performed by minimizing the cost function C, given by

$$\hat{m} = min_{\tilde{m}}(C) = min_{\tilde{m}}(\phi(\tilde{m}) + \alpha\psi(\tilde{m})) \qquad [2]$$

In the above equation, $\tilde{m}$ is the current image data estimate; $\phi(\tilde{m})$ is the data fidelity term; $\psi(\tilde{m})$ is the temporal constraint term (also known as a regularization term), which quantifies how well the reconstruction matches the temporal model; and α is the weighting factor or regularization parameter that determines how much to weight the constraint. The data fidelity term $\phi(\tilde{m})$ is given by

$$\phi(\tilde{m}) = \|WF\tilde{m} - \tilde{d}\|_2^2 \qquad [3]$$

where $\tilde{d}$ is the undersampled data in *k*-space, W is a binary sparsifying pattern (which represents the phase-encode lines that are sampled) to obtain $\tilde{d}$ from d, and $\|\cdot\|_2$ indicates the L_2 norm.

Depending on the kind of dynamic imaging data obtained, different temporal constraint terms for ψ can be chosen. For the current application, dynamic myocardial perfusion imaging, the temporal constraint chosen was based on the fact that for the complex image space data obtained from full k-space without motion, the time curves for each pixel are generally smoothly varying. Not only are the magnitude time curves smoothly varying, but the real and imaginary components also vary smoothly. This constraint was implemented with a maximum smoothness functional given by

$$\psi(\tilde{m}) = \sum_{i=1}^{N} \|\nabla_t \tilde{m}_i\|_2^2 \qquad [4]$$

In the above equation ∇_t is the temporal gradient operator, $\tilde{m}_i$ is the time curve for each pixel i in the estimated complex image space, and N is the total number of pixels in each time frame. The above model penalizes time curves with high temporal gradients, making the curves smooth in time.

Reconstruction was performed by minimizing the cost functional given by

$$\hat{m} = min_{\tilde{m}}[\|WF\tilde{m} - \tilde{d}\|_2^2 + \alpha \sum_{i=1}^{N} \|\nabla_t \tilde{m}_i\|_2^2] \qquad [5]$$

In Eq. [5] the final solution $\hat{m}$ is the set of all time curves that show a good balance between having fidelity to the measured data and satisfying the constraint term. The amount of temporal smoothness desired in the solution can be varied by changing α.

Minimization of the functional in Eq. [5] was performed using an iterative gradient descent approach with finite forward differences (20). The series of image frames were updated iteratively according to

$$\tilde{m}^{n+1} = \tilde{m}^n - \lambda C'(\tilde{m}^n); n = 0,1,2\cdots \qquad [6]$$

where λ corresponds to the step size of the gradient descent, n corresponds to the iteration number, and $C'(\tilde{m})$ corresponds to the Euler-Lagrange derivative of the functional in Eq. [5] with respect to $\tilde{m}$, given by

$$C'(\tilde{m}) = 2*(F^{-1}(WF\tilde{m}) - F^{-1}(\tilde{d}) - \alpha\nabla_t^2\tilde{m}) \qquad [7]$$

where ∇_t^2 represents the temporal Laplacian and operates on the complex data. The initial estimate for Eq. [6], $\tilde{m}^0$, was taken as the series of images obtained by computing the inverse 2D-FT on each time frame of acquired sparse data. Other initial estimates (e.g., all zeros) gave similar results; however, we note that methods such as the sliding-window technique can be used for initialization for faster convergence.

Choosing the appropriate weighting factor, α, for the temporal constraint term is important to obtain the best results for reconstruction. The weighting factor has to be chosen such that there is a good balance between the fidelity to the acquired data and satisfying the constraint. In this work the L-curve method proposed by Hansen (21) was used to determine the optimum weighting factor. The norm of the data fidelity term was plotted against the norm of the temporal constraint term on a log-log plot for different values of the weighting factors, and the optimum value of the weighting factor was given by the corner of the L-curve.

Acquisition

The reconstruction method using Eq. [5] was tested on perfusion data from four different patients with minimal respiratory motion. All patients provided informed consent in accordance with the University of Utah Institutional Review Board. Short-axis slices were acquired for every heartbeat in each patient on a Siemens 3T scanner using an eight-channel cardiac coil. Gd doses varied between 0.022 and 0.096 mmol/kg. A turbo fast low-angle shot (TurboFLASH) saturation recovery sequence with scan parameters TR = 140–175 ms, TE = 0.98–1.36 ms, and slice thickness = 7–8 mm was used. The acquisition matrix for different scans varied between (128–192) × (95–128). The acquired pixel size varied between (1.7–2.2) × (2.5–3) mm^2. Two of the datasets were obtained at rest and two were obtained during adenosine stress.

Full *k*-space data obtained from each coil were sparsified by selecting phase-encode lines in two different ways to determine which undersampling pattern performed better. An interleaved sampling fashion and a variable density (VD) sampling fashion were used. Figure 1a shows the interleaved sampling pattern of the full *k*-space data. In Fig. 1a the *k*-axis represents the phase-encode direction and the *t*-axis represents the time direction. The black dots represent the phase encodes that are kept. The frequency-encode direction is perpendicular to the plane of the paper. In the figure the data are sparsified by a factor of 4 (for the first time frame phase-encode lines 1, 5, 9. . . are chosen, for the second time frame phase-encode lines 2, 6, 10. . . are chosen, and so on).

Figure 1b shows the alternative sampling pattern using a VD pattern to sparsify the full *k*-space data. A few phase-encode lines around the center of *k*-space for each time frame are kept. Phase-encode lines further from the center on both sides are acquired with a lower acceleration factor, RL, in an interleaved fashion. The remaining *k*-space data are sampled in an interleaved fashion with a higher acceleration factor, RH. For the perfusion datasets four phase-encode lines around the center of *k*-space were sampled for each time frame, and four lines on either side were then sampled in interleaved fashion with RL = 2. The remaining data were sampled with higher accelerations in the interleaved fashion depending on the number of phase encodes, so that 20% of the full *k*-space data was sampled in total.

Analysis

Reconstruction using the TCR method was performed on the sparse data and the results were compared with those obtained using IFT reconstruction of full *k*-space data. Reconstructions from the TCR method were also compared with those obtained by the sliding-window (SW) reconstruction method from sparse data. In the SW reconstruction, a missing phase-encode line in a current time frame is replaced by using the corresponding phase encodes from the nearest-neighbor frame. Averaging of a phase encode from two different time frames was done if two nearest-neighbor frames had the same missing phase-encode line (11). The weighting factor for the temporal constraint term, α, was obtained using the L-curve method. Comparisons were made between the results obtained from a single coil and those obtained by combining the reconstructions from multiple coils with the square root of sum of squares (SOS). Root mean square error (RMSE) values were computed for the images reconstructed from sparse data by comparing them to the full data reconstructions using IFT. The mean signal intensity time curves for regions in the left ventricular (LV) blood pool and myocardium in the reconstructed images were compared with those obtained from full *k*-space data. SNRs and contrast-to-noise ratios (CNRs) for the reconstructed images were also compared. For a given dataset the SNR was computed for a single time frame, picked from the center of the perfusion sequence, according to $\frac{S_{LV}}{\sigma_{Noise}}$, where S_{LV} was obtained by computing the mean signal from a region in the LV blood pool, and σ_{Noise} was obtained by computing the standard deviation (SD) of noise from a region in the background. The CNR between the LV blood pool and myocardium was computed as $\frac{(S_{LV} - S_{Myo})}{\sigma_{Noise}}$, where S_{Myo} was obtained by computing the mean signal from a region in the myocardium on the time frame picked from the center of the temporal sequence.

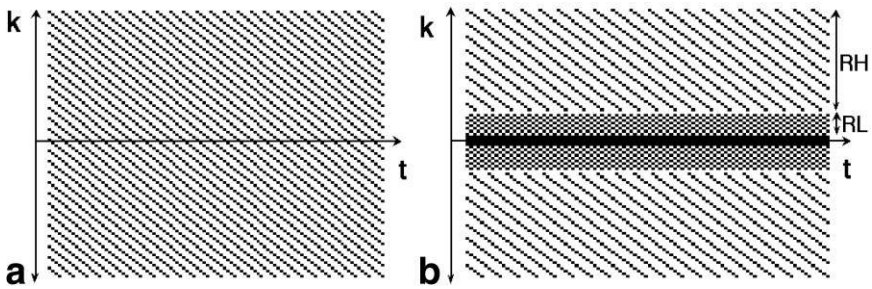

FIG. 1. **a:** Interleaved sparsifying pattern used to sample 25% of full *k*-space data. The *k*-axis represents the phase encodes and the *t*-axis represents the time frames. The frequency-encode direction is perpendicular to the plane of paper. The black dots represent the phase encodes sampled. **b:** *k*-*t* Space showing the VD sampling pattern. The *k*-axis represents phase encodes and the *t*-axis represents time. The frequency-encode direction is perpendicular to the plane of the paper. The black portion represents the data sampled. A few phase-encode lines around the center of *k*-space, represented by the black band in the center, are acquired for each time frame. Phase-encode lines a little further from the center on both sides are sampled in an interleaved fashion with an RL. The remaining phase-encode data are sampled with an RH in an interleaved fashion.

RESULTS

In this section, reconstructions obtained using the TCR method in Eq. [5] are presented. Interleaved, and VD sampling patterns are compared.

Interleaved Sampling

The sparsifying pattern in which phase-encode lines were removed in an interleaved fashion, as shown in Fig. 1a, was used to sample 25% of full data (R = 4). The reconstructed results are shown in Fig. 2. Figure 2a shows a time frame in a typical perfusion sequence obtained from full *k*-space data by using the IFT. Figure 2b shows the corresponding time frame reconstructed using the IFT on 25% of the full data. Figure 2c shows the corresponding time frame reconstructed using the SW technique. The arrow in the image points to a residual artifact in the reconstruction. Figure 2d shows the results of the TCR method obtained from sparse data. Figure 2e shows that for all of the time frames TCR has reduced RMSEs as compared to the SW method. Similar trends were seen when a region confined to the heart was used to calculate the RMSE. The SNR and CNR computed for the TCR-reconstructed image shown in Fig. 2d were 22.1 and 9.9, respectively, while the corresponding values reconstructed from full data using IFT were 18.3 and 8.3, respectively. Mean improvements of 27.4(±7.6)% in the SNR and 24.4(±7.1)% in the CNR were observed over the four datasets.

VD Sampling

Figure 3 shows the results obtained by using only 20% (R = 5) of full *k*-space data sparsified in the VD fashion on a dataset obtained during adenosine stress. Figure 3a shows two time frames reconstructed from a full dataset using the IFT. Figure 3b shows the corresponding time frames reconstructed from 20% of full *k*-space data using the SW method. The arrows in the time frames point to residual artifacts that are not resolved by the method. The corresponding time frames reconstructed using the TCR approach are shown in Fig. 3c. Figure 3d shows that the RMSE values for the sparse data reconstructions are always lower using TCR as compared to the SW method. Note that the R = 5 factor was achieved even though a full unaliased field of view (FOV) was not acquired initially.

Figure 4 compares the mean intensity time curves for different regions in the blood pool and myocardium for the TCR and SW reconstructions. Figure 4a shows a region in the LV blood pool, and the myocardium segmented into six equiangular regions. Figure 4b compares the mean intensity time curves for the region in the LV blood pool obtained from the images reconstructed from full data using IFT and images reconstructed from R = 5 data using the TCR and SW methods. Figure 4c–e compare the mean intensity time curves for region numbers 1, 2, and 6 in the myocardium, respectively. The time curves obtained from TCR matched with the full data reconstructions more closely than those obtained from the SW method.

The SNR and CNR values computed for the image reconstructed from sparse data using the TCR method were 18.6 and 11.8, respectively, while the corresponding values reconstructed from full data using the IFT were 16.5 and 10.1, respectively. For all of the four datasets reconstructed using the TCR method from data sparsified by a factor of 5 in the VD fashion, SNR and CNR values improved over those computed using the standard IFT reconstructions from full data. Mean improvements of 27.7(±4.3)% in SNR and 14.1(±3.7)% in CNR were observed.

Comparison of Interleaved and VD Sampling

Figure 5a shows the regions of interest (ROIs) defined in the LV blood pool and myocardium defined on a single time frame for the dataset in Fig. 3. The mean signal intensity time curves obtained from the regions in the LV blood pool region and the myocardium are compared in Fig. 5b and c, respectively. In Fig. 5b and c, the curve labeled "IFT recon-Full data" represents the mean intensity time curve obtained from images reconstructed from

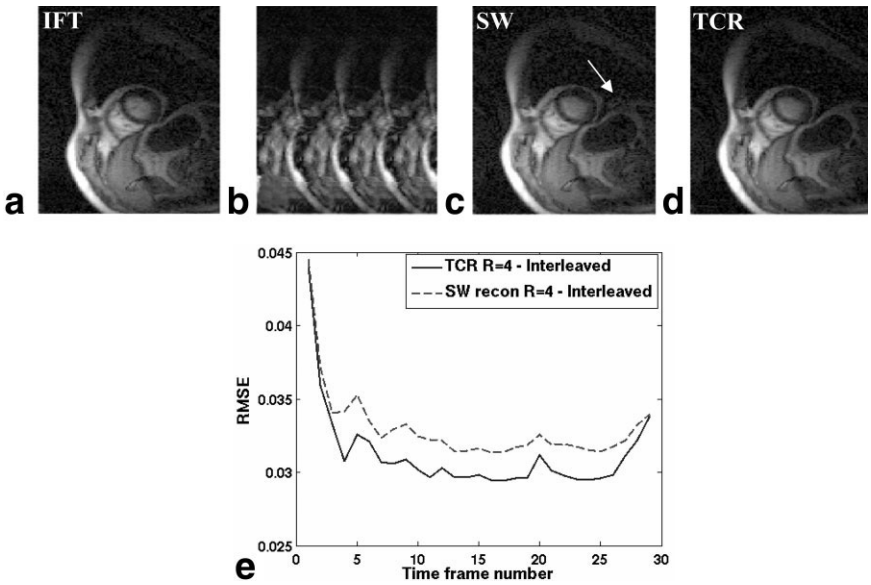

FIG. 2. Comparison of reconstructions from full data and R = 4 data using TCR and SW methods. **a:** A time frame reconstructed from full *k*-space data using IFT. **b:** Corresponding time frame reconstructed from sparse R = 4 data using the IFT. **c:** Corresponding time frame reconstructed using the SW technique. The arrow in the image points to residual artifacts in the SW method. **d:** Corresponding time frame reconstructed using the TCR method. The artifact present in c is reduced. **e:** Plot of RMSE values for each time frame computed for the SW and TCR methods.

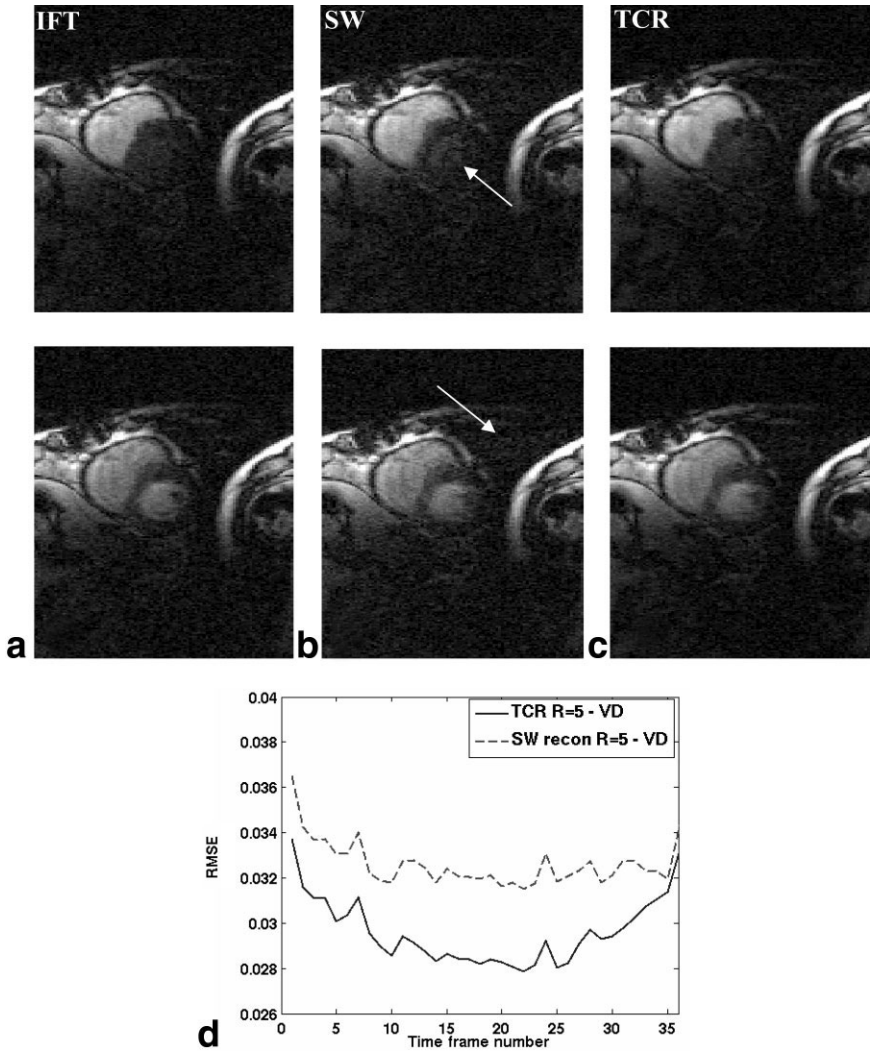

FIG. 3. Comparison of reconstructions from full data and R = 5 data using the TCR and SW methods. **a:** Two different time frames reconstructed from full *k*-space data using IFT (first column). **b:** Corresponding time frames reconstructed using SW technique. The arrows point to residual artifacts in the SW method (second column). **c:** Corresponding time frames reconstructed using TCR method. The artifacts present in b are reduced (third column). **d:** Comparison of RMSE values for each time frame computed for reconstructions from the SW and TCR methods.

full *k*-space data using the IFT, the curve labeled "TCR-VD" represents the mean intensity curve obtained from images reconstructed from 20% of full *k*-space data sampled in VD fashion using the TCR method, and the curve labeled "TCR-interleaved" represents the mean intensity curve obtained from images reconstructed from 20% of full data sampled in an interleaved fashion using the TCR method. The time curves obtained from data that are sparsified in VD fashion match well with those obtained from full data. The interleaved data did not reconstruct as well as the VD data when R = 5 was used.

Use of All Coils

The TCR method (Eq. [5]) was also applied independently to sparse data obtained from each of the eight coils. Full data from each coil were undersampled by a factor of 5 in VD fashion. The reconstructions from each coil were then combined using the SOS method, and the results for the dataset from Fig. 3 are shown in Fig. 6. Figure 6a shows zoomed versions of two time frames obtained from the SOS reconstructions from full data for each coil using the IFT, and Fig. 6b shows the corresponding time frames obtained from sparse data for each coil using the TCR approach. Figure 6c shows the corresponding difference images.

Weighting Factor

The L-curves obtained for sparse datasets (R = 4) from four patients are shown in Fig. 7. The norm of the data fidelity term (Eq. [3]) was plotted against the norm of the temporal constraint term (Eq. [4]) for different values of α. The optimum regularization parameter for each of the four datasets is close to 0.04.

To demonstrate the effect of different values of α, Fig. 8a shows an ROI defined in the LV blood pool on a single time frame of a perfusion dataset. Figure 8b–d compare the time curves obtained from the reconstructed sparse dataset (undersampled in VD fashion by a factor of 5) using Eq. [5] and choosing different values of α, and those obtained from full *k*-space data using the IFT. From the figures we see that choosing a value of α that is much less than the optimum value produces non-smooth time curves, while choosing a α value that is much greater than the optimum value produces overly smooth curves. More on the choice and robustness of α is included in the Discussion section below.

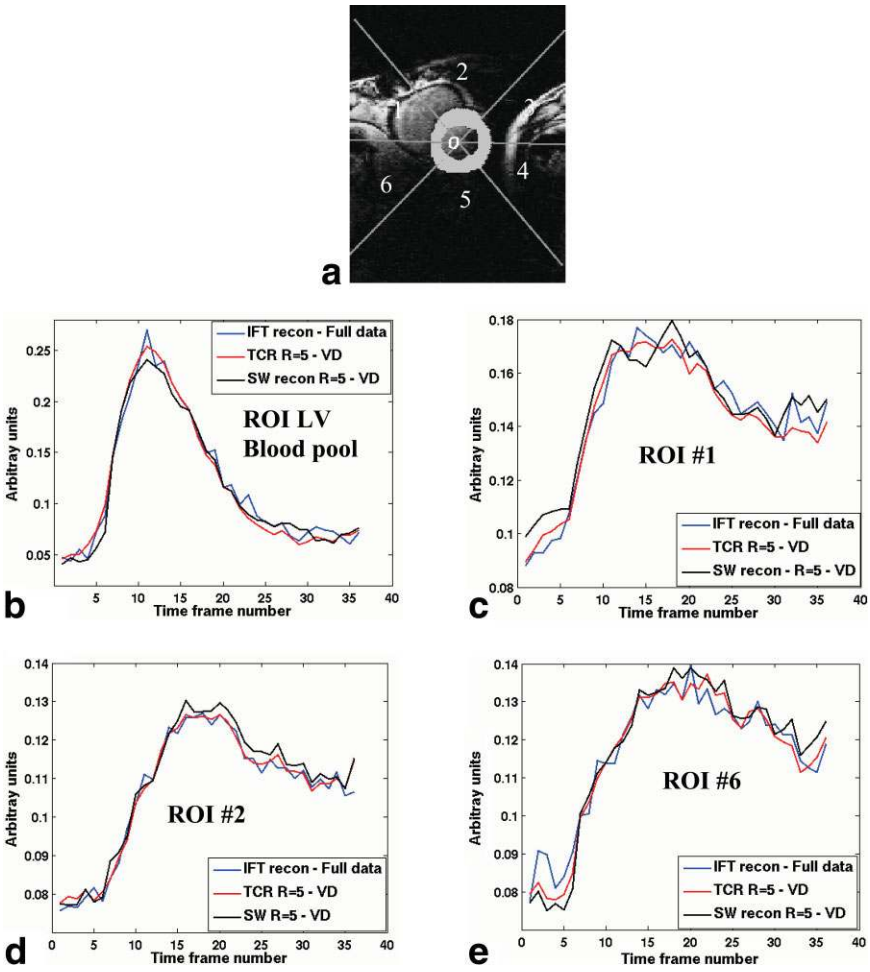

FIG. 4. Comparison of dynamics of reconstructions from TCR and SW for different regions in the blood pool and myocardium for the dataset shown in Fig. 3. **a:** Image showing an ROI in the LV blood pool and six segmented regions in the myocardium. The image was reconstructed from full data using the IFT from a single coil. **b:** Comparison of mean intensity time curves for the LV blood pool region shown in (a) for different reconstructions from full and sparse data (R = 5) undersampled in VD fashion. **c:** Comparison of mean intensity time curves for region 1 in the myocardium shown in (a) for different reconstructions. **d:** Comparison of mean intensity time curves for region 2 in the myocardium shown in (a) for different reconstructions. **e:** Comparison of mean intensity time curves for region 6 in the myocardium shown in (a) for different reconstructions.

DISCUSSION

An iterative TCR technique to reconstruct high-quality images from sparse *k*-space data has been presented. The method achieves high acceleration factors by using appropriate temporal model information. Since the method is based on temporal regularization of the complex image space data, it is robust to different sparsifying schemes with no additional computational burden.

Using complex data in the image space rather than magnitude data for the temporal constraint terms in the TCR method provides complementary information in terms of real and imaginary components of the data. For example, consider the maximum smoothness constraint in Eq. [4]. Figure 9a and c show the real and imaginary parts of a single time frame in complex image space, reconstructed from full *k*-space perfusion data. Figure 9b shows the mean signal intensity time curves for the LV blood pool region shown in Fig. 9a, obtained from the real part of complex image space reconstructed from full and sparse data using the IFT. Figure 9d shows the mean signal intensity time curves for the region in myocardium shown in Fig. 9c, obtained from the imaginary part of complex image

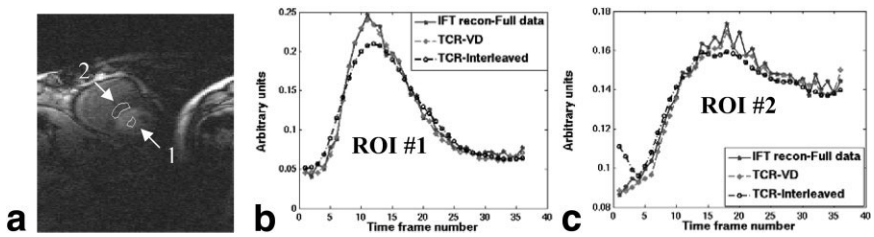

FIG. 5. Comparison of reconstructions from sparse data obtained using interleaved and VD sampling patterns. **a:** ROIs defined on a single time frame for the dataset in Fig. 3 in the LV blood pool and the myocardium. **b:** Comparison of average signal intensity time curves for the LV blood pool region shown in (a). **c:** Comparison of average signal intensity time curves for the region in the myocardium shown in (a). The reconstructions were obtained from full *k*-space data using IFT and compared with those obtained from 20% of full data sampled in VD and interleaved sampling patterns using the TCR approach in Eq. [5].

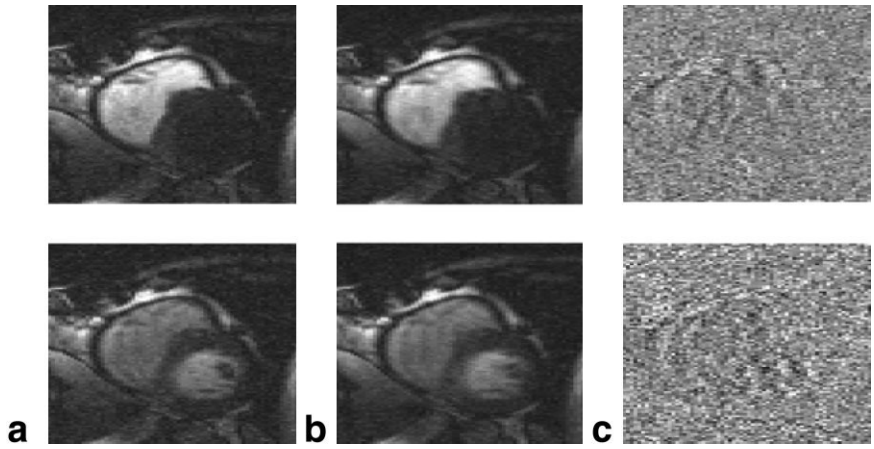

FIG. 6. Reconstruction results from all coils. The phase-encode direction is from left to right and the frequency-encode direction is from bottom to top. **a:** Zoomed image frames at two different time points in the perfusion dataset shown in Fig. 3, reconstructed using IFT from full *k*-space data for eight coils and combined using the SOS method (first column). **b:** Corresponding image frames reconstructed from 20% of full *k*-space data for each coil using the TCR approach. Full *k*-space data were sparsified by removing phase-encode lines in the VD fashion. Individual reconstructions from each coil were combined using the SOS method (second column). **c:** Corresponding difference images between (a) and (b) (third column). The images are scaled to highlight the differences.

space reconstructed from full and sparse data using the IFT. The sparse data were obtained by sampling 25% of the full *k*-space data in an interleaved fashion. The constraint in Eq. [4] is satisfied by the time curves for the pixels in the perfusion images for both real and imaginary parts, and the curves from the full data are smoother than those from the sparse data. Consistent with this, it was found that using the temporal constraint on complex image data performed better than using the constraint only on magnitude data.

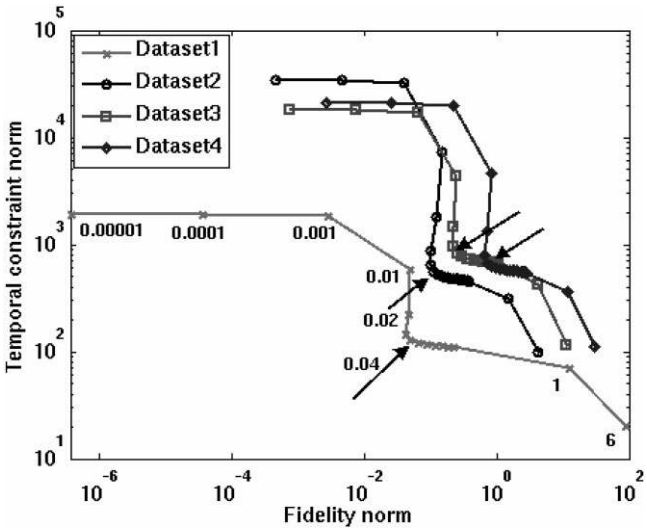

FIG. 7. L-curves for four different datasets shown on a log-log plot for different values of α. The temporal constraint norm corresponds to the norm in Eq. [4] and the data fidelity norm corresponds to the norm in Eq. [3]. The norms for datasets 2–4 are scaled to have a range similar to that of dataset 1 for illustrative purposes. The values of α are shown on the L-curve for dataset 1. The other datasets have the same α values, that is, the seventh sample point from the left corresponds to $\alpha = 0.04$. The arrows on the curves point to the corners of the L-curves, which are close to 0.04 for all four cases.

The temporal constraint used here is based on the assumption that there is little motion in the images. The results presented here were derived from rest and stress perfusion datasets with little respiratory motion (<2 pixels), where the method performs well. The method can be applied "as is" on patients with a good breath-hold, and is likely to be useful in other applications (e.g., DCE-MRI of some cancers) in which motion is not a significant issue.

Although some patients can maintain a good breath-hold, it can be difficult to obtain motion-free data, especially under stress perfusion. In the presence of respiratory motion, the TCR method was not able to fully resolve the artifacts from undersampling. This is likely due to the fact that motion combines with the adverse aliasing from the undersampling to produce complicated changes in the time curves that are not accurately regularized by the TCR method. The artifacts produced by motion are local in time, that is, the time frames with significant motion are affected more than those with less motion. Figure 10a shows a time frame reconstructed using IFT from full data that has some motion (~2 pixels in both the *x* and *y* directions) in the heart region as compared to its adjacent time frames, and Fig. 10b shows the corresponding time frame reconstructed from R = 4 data with TCR. Figure 10c shows the corresponding difference image between Fig. 10a and b. Figure 10d shows a different time frame later in the sequence reconstructed using IFT from full data in which there is motion in the chest wall (~3 pixels) and heart region (~2 pixels) as compared to its adjacent time frames. The chest wall and heart region are moving in different directions. Figure 10e shows the corresponding time frame reconstructed from R = 4 data with TCR. Figure 10f shows the difference image between Fig. 10d and e. We can see that artifacts from the undersampling are more

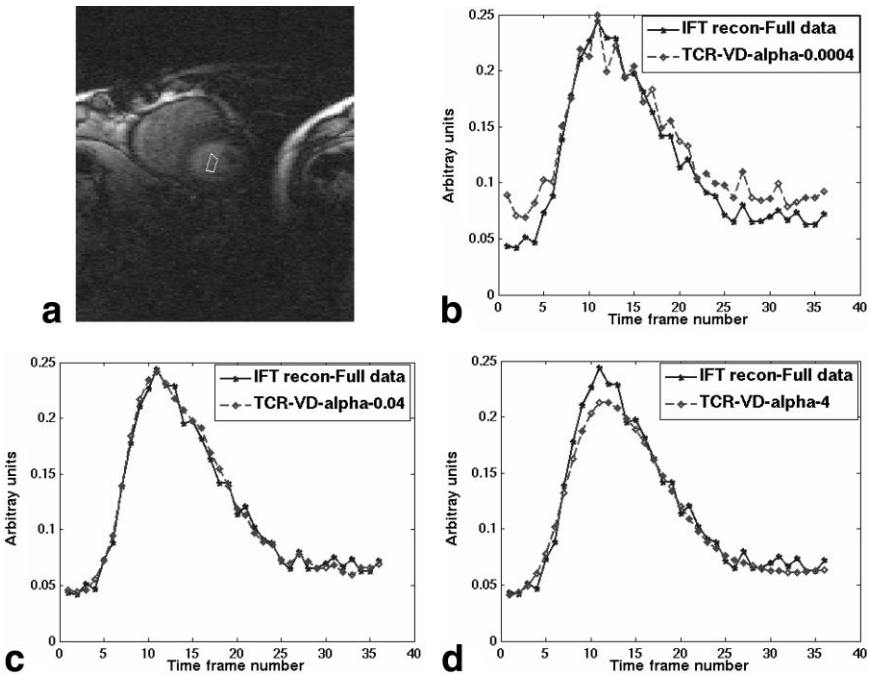

FIG. 8. Comparison of results of reconstruction using the TCR approach with different values of α. **a:** ROI defined in the LV blood pool on a single time frame reconstructed using IFT from full *k*-space data of the perfusion dataset in Fig. 3. **b–d:** Comparison of the mean intensity time curves for the region shown in a obtained from the images reconstructed using IFT from full data, and using TCR from 20% of the full data sampled in VD fashion for $\alpha = 0.0004$, $\alpha = 0.04$, and $\alpha = 4$, respectively.

significant in the time frame with motion in both the chest wall and heart regions.

Incorporating motion-related issues in the TCR method is not addressed here, and will be the subject of future work. Artifacts arising from motion can be reduced by incorporating a priori determined information about the motion into the reconstruction. One method to handle respiratory motion is to use calibration scans to identify the motion of the chest wall and other anatomy from a training dataset, and then to correlate the movements with signals from a real-time navigator or respiratory belt so that motion is measured.

The TCR method was tested by downsampling full *k*-space data. While this simulates an acquisition with $R = 5$, actual data acquisition with $R = 5$ has not been tested. This type of downsampling may not provide a true fivefold acceleration depending on the pulse sequence used. To achieve the reported R-values for cardiac saturation recovery sequences, pulse sequences such as those proposed in Refs. 22 and 23 should be used to acquire sparse data for

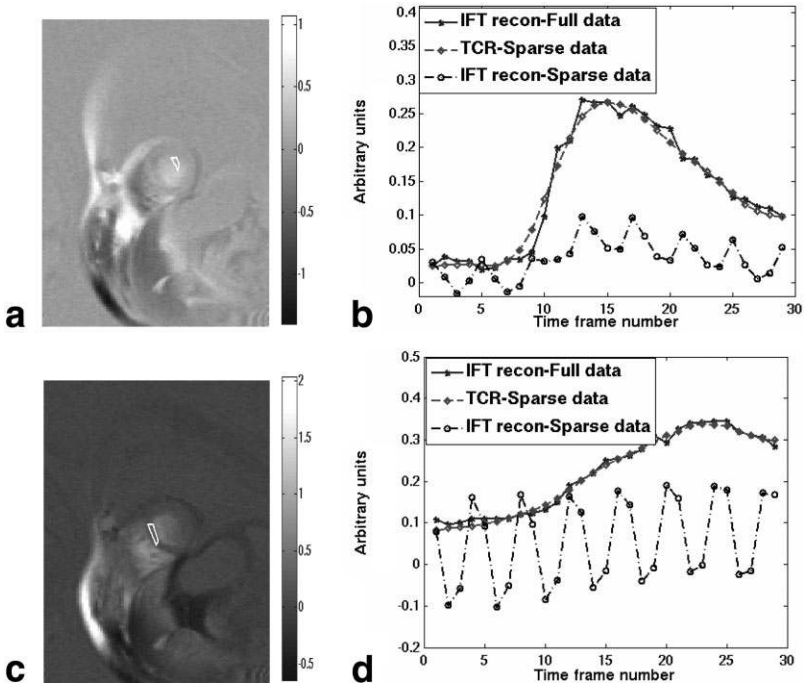

FIG. 9. Comparison of time curves from real and imaginary parts of reconstructed complex image space obtained from full *k*-space data and sparse data undersampled by a factor of 4 in interleaved fashion. **a:** Real part of a single time frame in complex image space reconstructed from full *k*-space data using IFT with an ROI in the LV blood pool. **b:** Comparison of the mean intensity time curves for the region shown in (a) for the real part of the complex image data reconstructed from full *k*-space using IFT, 25% of full *k*-space data using IFT, and the TCR approach in Eq. [5]. **c:** Imaginary part of the corresponding time frame in complex image space reconstructed from full *k*-space data using IFT with an ROI in the myocardium. **d:** Comparison of the mean intensity time curves for the region shown in c for the imaginary part of the complex image data reconstructed from full *k*-space using IFT, 25% of full *k*-space data using IFT, and the TCR approach in Eq. [5].

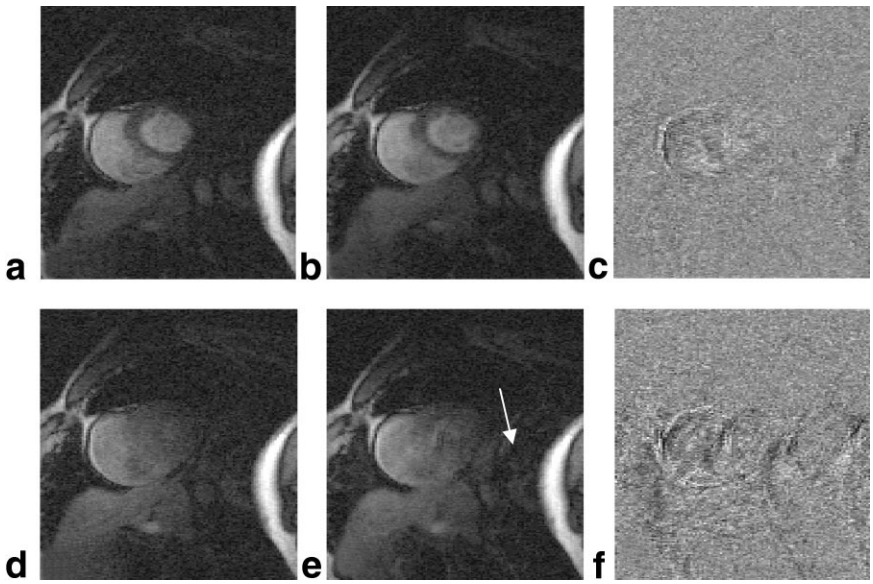

FIG. 10. Example of the effect of respiratory motion on the TCR method. **a:** A time frame in a perfusion sequence reconstructed from full data using IFT, which has motion of ~2 pixels in the *x* and *y* directions in the heart region as compared to its adjacent frames. **b:** Corresponding time frame reconstructed from R = 4 data (interleaved undersampling) using the TCR method. **c:** Image showing the difference between (a) and (b). **d:** A different time frame later in the sequence reconstructed from full data using IFT, which has motion of ~3 pixels in the chest wall in *x* direction and ~2 pixels in the *x* and *y* directions in the heart region as compared to its adjacent frames. **e:** Corresponding time frame reconstructed using the TCR method. The arrow points to the residual artifacts that are not resolved by TCR. **f:** Corresponding difference image between (d) and (e).

multiple slices. This issue is independent of the type of reconstruction used.

More complex temporal models, such as B-splines or a two-compartment model, can also be used as temporal constraints to achieve high acceleration factors. Alternatively, one can estimate the parameters of such temporal models, rather than estimating every pixel value at every time point. We recently applied a two-compartment model to reconstruct parameterized images from simulated data (24).

The TCR technique is independent of coil configurations and hence can be used in conjunction with parallel imaging techniques (14,15) to achieve higher accelerations or to further improve the quality of images. Unlike parallel imaging techniques, which impose an SNR penalty on the reconstructed images, the TCR method improves SNR over the standard IFT reconstructions by taking advantage of the temporal data correlations.

Although the TCR approach is robust to different sparsifying schemes, we observed that a higher acceleration (R = 5) for Cartesian undersampling could be achieved using a VD sampling pattern, compared to R = 4 for the interleaved sampling pattern. Figure 5b and c compare the time curves for the regions shown in Fig. 5a reconstructed from sparse data obtained using interleaved and VD sampling. The curves obtained using the VD sampling pattern match better with those obtained from full *k*-space data. This is reasonable since the contrast dynamics are mostly captured by the lines around the center of *k*-space, and the high-frequency information can be captured very sparsely over a number of time frames.

Determining the optimum weighting factor for the constraint on each dataset using the L-curve method is time-consuming due to the computation of the norms of the solutions for different values of α. However, from the L-curves for the four datasets in Fig. 7, the weighting factor does not vary significantly for different datasets, and a fixed value can likely be used. Also, we found that the TCR method was robust to perturbations ($\pm 0.5\alpha$) in the optimum value of α. This implies that in practice, a fixed value of α will be useful for all myocardial perfusion datasets acquired in this manner. Even better performance may be possible with a spatially adaptive α parameter that is tailored to reflect how dynamic different regions are expected to be.

For all of the datasets, a fixed number of iterations (1000) of gradient descent was empirically chosen to minimize the TCR functional in Eq. [5]. We found that the cost functional in Eq. [5] dropped significantly in the first few iterations and dropped at a slower rate for the later iterations. Figure 11 shows the plot of the $\log_e$(cost) and the total RMSE values (scaled) computed for all of the time frames vs. the number of iterations. We can see that the RMSE values also drop significantly in the first few iterations, but do not change significantly for later iterations.

Matlab (The Mathworks, Natick, MA, USA) implementations for the TCR in Eq. [5] took about 7 min on a

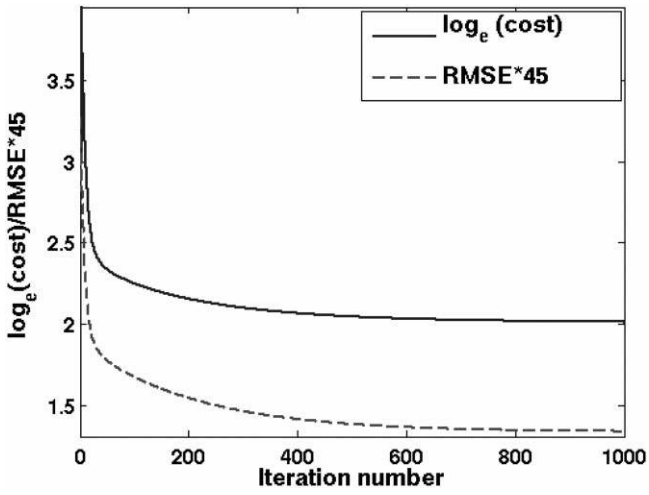

FIG. 11. Plots comparing the $\log_e$(cost function) in Eq. [5] and total RMSE values (scaled) for all time frames as a function of the iteration number.

machine with an AMD dual core processor and 4GB RAM to reconstruct a dataset containing 36 time frames from 20% of full data sampled with the VD pattern. TCR was also implemented using C++ in the ITK (25) framework and gave equivalent results.

CONCLUSIONS

The TCR method was used to reconstruct sparse dynamic data, which could allow improved coverage or improved spatial or temporal resolution. The method achieved accelerations up to a factor of 5 while preserving the quality of myocardial perfusion datasets that had little respiratory motion. A mean improvement of 27.7(±4.3)% in SNR and 14.1(±3.7)% in CNR between the LV blood pool and the myocardium was observed. The method can be extended to improve the acquisition speed of other DCE imaging techniques, such as DCE tumor imaging, where assumptions regarding the temporal characteristics of the data can be similar to the contrast kinetics in the heart.

ACKNOWLEDGMENTS

We appreciate the help of Chris McGann, M.D., Henry Buswell, Melody Johnson, and Nate Pack with data acquisition.

REFERENCES

1. Van Vaals JJ, Brummer ME, Dixon TW, Tuithof HH, Engels H, Nelson C, Gerety BM, Chezmar JL, den Boer JA. "Keyhole" method for accelerating imaging of contrast agent uptake. J Magn Reson Imaging 1993;3:671–675.
2. Jones RA, Haraldseth O, Muller TB, Rinck PA, Oksendal AN. k-Space substitution: a novel dynamic imaging technique. Magn Reson Med 1993;29:830–834.
3. Webb AG, Liang Z-P, Magin RL, Lauterbur PC. Application of reduced-encoding MR imaging with generalized-series reconstruction (RIGR). J Magn Reson Imaging 1993;3:925–928.
4. Chandra S, Liang Z-P, Webb A, Lee H, Morris D, Lauterbur PC. Application of reduced-encoding imaging with generalized-series reconstruction (RIGR) in dynamic MR imaging. J Magn Reson Imaging 1996;6:783–797.
5. Hanson JM, Liang Z-P, Wiener EC, Lauterbur PC. Fast dynamic imaging using two reference images. Magn Reson Med 1996;36:172–175.
6. Riederer SJ, Tasciyan T, Farzaneh F, Lee JN, Wright RC, Herfkens RJ. MR fluoroscopy: technical feasibility. Magn Reson Med 1988;8:1–15.
7. Parrish T, Hu X. Continuous update with random encoding (CURE): a new strategy for dynamic imaging. Magn Reson Med 1995;33:326–336.
8. Doyle M, Walsh EG, Blackwell GG, Pohost GM. Block regional interpolation scheme for k-space (BRISK): a rapid cardiac imaging technique. Magn Reson Med 1995;33:163–170.
9. Zaitsev M, Zilles K, Shah NJ. Shared k-space echo planar imaging with keyhole. Magn Reson Med 2001;45:109–117.
10. Madore B, Glover GH, Pelc NJ. Unaliasing by Fourier-encoding the overlaps using the temporal dimension (UNFOLD), applied to cardiac imaging and fMRI. Magn Reson Med 1999;42:813–828.
11. Tsao J, Boesiger P, Pruessmann KP. k-t BLAST and k-t SENSE: dynamic MRI with high frame rate exploiting spatiotemporal correlations. Magn Reson Med 2003;50:1031–1042.
12. Kozerke S, Tsao J, Razavi R, Boesiger P. Accelerating cardiac cine 3D imaging using k-t BLAST. Magn Reson Med 2004;52:19–26.
13. Jahnke C, Paetsch I, Gebker R, Bornstedt A, Fleck E, Nagel E. Accelerated 4D dobutamine stress MR imaging with k-t BLAST: feasibility and diagnostic performance. Radiology 2006;241:718–728.
14. Sodickson DK, Manning WJ. Simultaneous acquisition of spatial harmonics (SMASH): fast imaging with radiofrequency coil arrays. Magn Reson Med 1997;38:591–603.
15. Pruessmann KP, Weiger M, Scheidegger MB, Boesiger P. SENSE: sensitivity encoding for fast MRI. Magn Reson Med 1999;42:952–962.
16. Kellman P, Epstein FH, McVeigh ER. Adaptive sensitivity encoding incorporating temporal filtering (TSENSE). Magn Reson Med 2001;45:846–852.
17. Kozerke S, Tsao J. Reduced data acquisition methods in cardiac imaging. Top Magn Reson Imaging 2004;15:161–168.
18. Hansen MS, Kozerke S, Pruessmann KP, Boesiger P, Pedersen EM, Tsao J. On the influence of training data quality in k-t BLAST reconstruction. Magn Reson Med 2004;52:1175–1183.
19. Portniaguine O, Bonifasi C, DiBella EVR, Whitaker RT. Inverse methods for reduced k-space acquisition. In: Proceedings of the 11th Annual Meeting of ISMRM, Toronto, Canada, 2003 (Abstract 481).
20. Karniadakis GEM, Kirby II RM. Parallel scientific computing in C++ and MPI. Cambridge: Cambridge University Press; 2003.
21. Hansen PC. 2001. The L-curve and its use in the numerical treatment of inverse problems. In: Johnston P, editor. Computational Inverse Problems in Electrocardiology. Southampton, UK: WIT Press. 119–142.
22. Slavin GS, Wolff SD, Gupta SN, Foo TKF. First-pass myocardial perfusion MR imaging with interleaved notched saturation: feasibility study. Radiology 2001;219:258–263.
23. Kellman P, Derbyshire JA, Agyeman KO, McVeigh ER, Arai AE. Extended coverage first pass perfusion imaging using slice interleaved TSENSE. Magn Reson Med 2004;51:200–204.
24. Awate SP, DiBella EVR, Tasdizen T, Whitaker RT. Model-based reconstruction for dynamic cardiac perfusion MRI from sparse data. In: Proceedings of the 28th Annual Meeting of IEEE EMBC, New York, NY, USA, 2006. p 936–941.
25. Yoo TS, Ackerman MJ, Lorensen WE, Schroeder W, Chalana V, Aylward S, Metaxas D, Whitaker RT. Engineering and algorithm design for an image processing API: a technical report on ITK—the Insight Toolkit. Studies Health Technol Inform 2002;85:586–592.